



# Scaffold printing using biodegradable poly(1,4-butylene carbonate) ink: printability, *in vivo* physicochemical properties, and biocompatibility



Y.B. Ji<sup>a,c</sup>, J.Y. Park<sup>a,c</sup>, Y. Kang<sup>a</sup>, S. Lee<sup>a</sup>, H.J. Ju<sup>a</sup>, S. Choi<sup>a</sup>, B.Y. Lee<sup>a,\*\*</sup>, M.S. Kim<sup>a,b,\*</sup>

<sup>a</sup> Department of Molecular Science and Technology, Ajou University, Suwon 16499, South Korea

<sup>b</sup> Research Institute Center, Medipolymers, Research Institute, Suwon 16522, South Korea

## ARTICLE INFO

### Keywords:

Printing ink  
Aliphatic polycarbonate  
3D-scaffold  
*In vivo* biodegradation  
*In vivo* neo-tissue formation

## ABSTRACT

This study is the first to assess the applicability of biodegradable poly(1,4-butylene carbonate) (PBC) as a printing ink for fused deposition modeling (FDM). Here, PBC was successfully prepared via the bulk polycondensation of 1,4-butanediol and dimethyl carbonate. PBC was melted above 150°C in the heating chamber of an FDM printer, after which it flowed from the printing nozzle upon applying pressure and solidified at room temperature to create a three-dimensional (3D) scaffold structure. A 3D scaffold exactly matching the program design was obtained by controlling the temperature and pressure of the FDM printer. The compressive moduli of the printed PBC scaffold decreased as a function of implantation time. The printed PBC scaffold exhibited good *in vitro* biocompatibility, as well as *in vivo* neotissue formation and little host tissue response, which was proportional to the gradual biodegradation. Collectively, our findings demonstrated the feasibility of PBC as a suitable printing ink candidate for the creation of scaffolds via FDM printing.

## 1. Introduction

Developing living functional tissues through artificial means may one day cover the currently unmet demand for tissue replacement and organ transplantation [1]. Three-dimensional (3D) printing is a state-of-the-art technology that enables the fabrication of organs with a hierarchical architecture similar to that of their native counterparts [2].

Printing is essentially a rapid prototyping or additive manufacturing technique through which biological organs can be printed in a layer-by-layer fashion [3–7]. Additive manufacturing techniques include stereolithography, inkjet printing, fused deposition modeling (FDM), selective laser sintering (SLS), and digital laser printing (DLP), among others.

Among these printing strategies, FDM offers an inexpensive means to create scaffolds with controlled porosity and architecture using commercially available and biodegradable polymers. In FDM printing, a printing ink prepared from a given biomaterial leaves the print head in liquid form, after which it is printed layer by layer and solidifies to retain its shape until the entire organ is complete [8–10]; nevertheless, it is worth mentioning that FDM printing cannot be performed *in situ* (i.e., directly in living organisms) because of the extremely high extrusion temperatures required by this technique [11].

3D printed scaffolds are biocompatible, biodegradable, and allow for cellular responses and tissue formation when applied *in vivo* [12]. In addition, 3D printed scaffold with interconnected pores and large surface areas can support cell attachment, growth, intercellular communication, and gas/nutrient exchange, all of which are important advantages over the traditional salt leaching, phase separation, and melt molding techniques [5,13,14].

Polymers are widely used biomaterials for FDM printing, and polymers used as printing ink can be both natural or synthetic [15,16]. Furthermore, the polymers can also be biodegradable or nondegradable. Therefore, printed scaffolds using biodegradable polymers are especially well-suited for use in living organisms and are therefore more widely used.

Therefore, degradable biomaterials such as polyesters, poly( $\alpha$ -hydroxy acids), polylactones, polyorthoesters, and polyanhydrides are often used as printing ink for scaffold printing [17–20].

Among these polymers, aliphatic polycarbonates such as poly(ethylene carbonate) and poly(trimethylene carbonate) have recently garnered increasing attention due to their applicability as biodegradable polymers [5,12–25].

Particularly, polycarbonates form diols and carbon dioxide when degraded *in vitro* and *in vivo*, making this a generally safe and

\* Corresponding author.

\*\* Corresponding author.

E-mail addresses: [bunyeoul@ajou.ac.kr](mailto:bunyeoul@ajou.ac.kr) (B.Y. Lee), [moonskim@ajou.ac.kr](mailto:moonskim@ajou.ac.kr) (M.S. Kim).

<sup>c</sup> Y.B.J. and J.Y.P. contributed equally to this work.

noncytotoxic material. Therefore, polycarbonates have been implemented in several biomedical applications, such as drug and cell carriers [26].

However, to the best of our knowledge, no previous studies have described the use of biodegradable polycarbonates as a printing ink. Recently, we successfully prepared high-molecular-weight aliphatic poly(1,4-butylene carbonate) (PBC) via condensation polymerization of aliphatic 1,4-butanediol with dimethyl carbonate [27]. The melting temperature ( $T_m$ ) of the PBC prepared herein ranged between 140 and 160°C. This ability to flow within the aforementioned temperature range and then solidify makes PBC a uniquely well-suited printing ink material for FDM printing.

Nonetheless, innovative tissue engineering using printing currently faces several challenges, including the development of (1) biocompatible and printable ink that allows for prompt cell attachment and proliferation, (2) ink to adjust the mechanical integrity of printed scaffolds until full remodeling and regeneration, and (3) ink with low immunogenic reaction.

Therefore, the objectives of this study were to (1) assess whether printability (the flowing, solidification, and formation of designed shape) of PBC could be effectively implemented in FDM printing, (2) determine whether the printed PBC scaffolds could effectively maintain or modulate *in vivo* physicochemical properties (compress modulus and biodegradation) over a defined experimental period, and (3) evaluate whether the printed PBC scaffolds induced *in vivo* biocompatibility (Fig. 1). Therefore, our study provides important insights into the potential applicability of PBC as a suitable ink candidate for FDM-based scaffold printing.

## 2. Experimental section

### 2.1. Synthesis of aliphatic PBC

PBC was prepared via the bulk polycondensation of 1,4-butanediol (10.0 g, 111 mmol) and dimethyl carbonate (15.7 g, 174 mmol) as described previously [27]. The resulting PBC was then characterized using  $^1\text{H}$  NMR (JNM-ECZ 600 MHz NMR spectrometer; JEOL, Tokyo, Japan).  $^1\text{H}$  NMR chemical shifts were monitored using tetramethylsilane in  $\text{CDCl}_3$  as an internal standard. In the  $^1\text{H}$  NMR spectrum of  $\text{CDCl}_3$ , two peaks (i.e., those corresponding to  $-\text{CH}_2\text{O}-$  and  $-\text{CH}_2\text{CH}_2\text{O}-$ ) were observed at 4.5–4.1 and 2.1–1.7 ppm, with equal integration values.

The molecular weight (MW) distribution of PBC was determined via gel

permeation chromatography (GPC) using a Futecs GPC 500 system coupled with a Shodex 201H RI detector (Futecs, Daejeon, Korea) and polystyrene gel columns (Shodex K-802, K-803, and K-804) in  $\text{CHCl}_3$  at 40°C as an eluent at a flow rate of 1 mL/min. Polystyrene standards were used to calibrate and determine the relative MW and the distribution of MW of PBC.

The melting point and thermal decomposition of PBC were determined through differential scanning calorimetry (DSC) and thermogravimetric analysis (TGA), respectively, using a TA instruments Q10 series model system (TA instruments, New Castle, USA) at a 5°C/min heating rate in the presence of nitrogen.

### 2.2. Thermal analysis of PBC

To evaluate the thermal stability of PBC in a heating chamber as printing ink, 1 g of PBC was heated in a heating oven at a preset temperature for 6 h. Afterward, GPC measurements were performed to monitor MW changes, as described in Section 2.1.

### 2.3. Fabrication of a PBC scaffold via FDM printing

PBC scaffolds were printed using an FDM 3D plotter system (Protek Korea, Daejeon, Korea) equipped with a heating jacket and a stainless-steel cylinder with a micronozzle. The micronozzle was moved with an air dispenser in the  $x$ - $y$ - $z$  stage axes. The plotting system was controlled using the Scaffold Path Generation SW computer software (Korea Institute of Machinery and Materials, Daejeon, Korea). PBC was added to the stainless-steel barrel of the heating jacket and then heated at 150–240°C for 30 min. The melted PBC was extruded from a micronozzle with an internal diameter of 400  $\mu\text{m}$  with pressurized air (100–500 kPa) at an output speed of 15 mm/s. The first PBC layer was printed as a series of parallel lines along the  $y$ -direction, whereas the second layer was deposited along the  $x$ -direction. The third and fourth layers were applied using the same deposition procedure. Using this procedure, printed PBC scaffolds (10 mm width  $\times$  10 mm length  $\times$  3 mm height) were obtained.

The effects of a micronozzle output speed (10, 15, and 20 mm/s), line shift (0, 25, and 50%), chamber temperature (150–240°C) and extrusion pressure (100–500 kPa) variations on PBC printability were also examined. Afterward, the printed scaffolds were compared with the original design in the program, including the line thickness and pores based on the  $x$ -

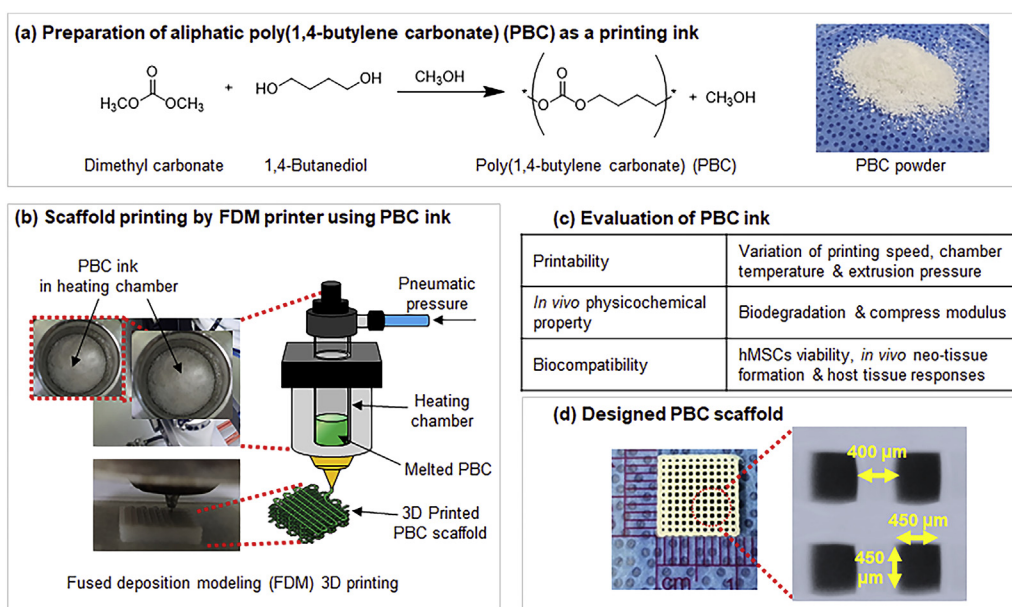


Fig. 1. Schematic of (a) preparation of poly(1,4-butylene carbonate) (PBC), (b) scaffold printing by the fused deposition modeling (FDM) 3D printing process using a PBC ink, and (c) evaluation of PBC ink and (d) images of the designed PBC scaffold.

length, to determine the printability of PBC. The designed scaffold was printed layer by layer with a line diameter of 400  $\mu\text{m}$  and a sectional length and width of 450  $\times$  450  $\mu\text{m}^2$ . The printed PBC scaffolds were sterilized via ultraviolet irradiation for 24 h for downstream experiments. The sterilized PBC scaffold maintained its original shape.

#### 2.4. Comparison of cell proliferation on printed PBC scaffolds

Cryopreserved bone marrow-derived mesenchymal stem cells (PCS-500-012, Normal, Human; hMSCs) were purchased from ATCC (Manassas, VA, USA). The cells were cultured in a cell culture flask in Dulbecco's modified Eagle's medium supplemented with 1% fetal bovine serum (Hyclone, New Zealand), 100 U/mL penicillin, and 100 mg/mL streptomycin for the subsequent experiments.

To evaluate the biocompatibility of the printed PBC scaffolds, half of the total hMSCs (passage number 7,  $1 \times 10^4$  cell/scaffold) were loaded on the top side of the PBC scaffold and then incubated for 1 h. Afterward, the remaining half of the hMSCs was loaded on the opposite side of the first scaffold. The hMSC-loaded PBC scaffold was then cultured on 24-well plates for 1, 4, and 7 days at 37°C in a 5% CO<sub>2</sub> incubator. The hMSC-loaded PBC scaffolds were then transferred to fresh 24-well plates to perform the WST-1 assay. As a control, equal numbers of hMSCs were cultured in 24-well plates without any additional treatment. hMSC attachment and proliferation were measured using the WST-1 kit. Afterward, 100  $\mu\text{L}$  of the WST-1 reagent was added to 24-well plates containing hMSCs and incubated at 37°C for 4 h. Then, 100  $\mu\text{L}$  was aliquoted from each well and transferred to a 96-well plate. The absorbance intensity of the solution was measured at 450 nm using a microplate reader. The absorbance intensity of hMSCs in the culture plate and PBC scaffold were individually determined and plotted over time to compare hMSC attachment and proliferation.

For scanning electron microscopy (SEM) analysis, the hMSCs on the printed PBC scaffolds were washed with Dulbecco's phosphate-buffered saline three times and then treated with 2.5% glutaraldehyde solution overnight. The hydration of scaffolds were performed by immersing the slides for 20 min with each different ethanol solution (60%, 70%, 80%, 90%, and 100%) and then were freeze dried at -75°C. The dried PBC scaffolds were coated with a thin layer of gold using a plasma sputter apparatus (Cressington; Redding, CA, USA) in the presence of argon gas. The morphology of the hMSCs on the PBC scaffolds was visualized using a JSM-6380 scanning electron microscope (JEOL, Tokyo, Japan).

#### 2.5. Animal implantation surgery

All experiments were conducted using healthy Sprague-Dawley rats (280–300 g, aged 6 weeks, male). All experimental protocols involving live animals were approved by the Institutional Animal Care and Use Committee of Ajou University (approval no. 2012-0004). Similarly, *in vivo* experiments were conducted in accordance with guidelines approved by the Animal Ethics Committee for Care and Use of Laboratory Animals of the Ajou University Medical Center.

The Sprague-Dawley (SD) rats were anesthetized with a Zoletil® and Rompun® (1:1) solution at a 1.5 mL/kg dose. The backsides of the anesthetized SD rats were shaved and sterilized with povidone, after which 2–3 cm of subcutaneous backside tissue was excised. The sterilized scaffolds were then transplanted into the subcutaneous backside. At 4, 8, and 16 weeks, the SD rats were euthanized with CO<sub>2</sub> gas. The PBC scaffolds were then excised from the implantation sites. Three PBC scaffolds removed from rats at each time point were used for GPC, NMR, SEM, and histological analyses.

#### 2.6. Optical and SEM image observation of *in vivo* implanted PBC scaffolds

The optical images of the PBC scaffolds removed from SD rats were first acquired using a Camscope system (Sometech, Seoul, Korea) at a 100 $\times$  and 400 $\times$  magnification. SEM images of PBC scaffolds removed

from SD rats were acquired and analyzed at a 50 $\times$  and 100 $\times$  magnification using SEM, as described in Section 2.4.

#### 2.7. Evaluation of the mechanical properties of *in vivo* implanted PBC scaffolds

To observe the changes in strength according to the implantation time, the compressive modulus of the PBC scaffolds removed from SD at 4, 8, and 16 weeks was measured using an H5KT universal testing machine (Tinius-Olsen, Horsham, PA, USA). The tissue adhered to the surface of the excised PBC scaffolds was removed as much as possible with scissors to eliminate measurement biases; however, the internal tissue on the excised PBC scaffolds was maintained unaltered to confirm the changes in mechanical properties because of the neotissue formation. Week 0 represents the original PBC scaffold. Measurements were performed at a load speed of 1 mm/min using a 500 N load cell sensor.

#### 2.8. Biodegradation evaluation of *in vivo* implanted PBC scaffold

The PBC scaffolds removed from SD rats were suspended in 5 mL of chloroform and pulverized with a homogenizer at 25°C and 4,000 rpm for 10 min. The mixture was sonicated at 25°C for 30 min, then centrifuged at 25°C and 4,000 rpm for 10 min. The suspension was then filtered with a PTFE filter and dried under low pressure to remove the chloroform. The dried mixtures were precipitated in *n*-hexane and ethyl ether (4:1), thus separating into soluble and insoluble portions. The soluble portion was filtered with filter paper and then freeze dried for 3 days, whereas the insoluble portion was simply freeze dried for 3 days. Equal concentrations of the dried portions of the PBC scaffolds removed at each implantation time were measured via <sup>1</sup>H NMR and GPC.

At predetermined time intervals, the weight-average molecular weights of the dried portions of the *in vivo* PBC scaffolds were determined at GPC peak calibrated based on the polystyrene standards. The weight-average molecular weight was determined by calibration of the polystyrene standards. The weight-average molecular weight at GPC peak was used to determine the change of relative MW at the predetermined time points. In addition, the line diameters were determined in an LSM 710 microscope to determine the change of relative degradation at the predetermined time points.

The degradation ratio was defined as follows: degradation ratio (%) = [MW determined at the GPC peak or line diameters at the predetermined time points/MW determined at the GPC peak or line diameters on week 0]  $\times$  100.

#### 2.9. Histological analysis of *in vivo* implanted PBC scaffolds

The PBC scaffolds removed from SD rats were immersed in 10% formalin for 2 days and fixed to prepare a paraffin block. The paraffin block was cut into 5  $\mu\text{m}$  sections, attached to the slide, and dried for 1 h. The samples were then heated at 70°C to remove the paraffin. Deparaffinization and hydration was performed by immersing the slides for 5 min in two times, ethanol 100% two times, ethanol 95% one time, and ethanol 70% one time. Afterward, the samples were treated with a hematoxylin solution for 3 min, washed with running water, then treated with eosin for 6 min, and once again washed with running water to obtain H&E-stained images. After drying the slide for 3 h at room temperature, the slides were mounted with a mounting solution. Neotissue formation on the H&E-stained images was observed using a slide scanner (ZEISS Axio Scan. Z1, Carl Zeiss Microscopy GmbH, Jena, Germany) and analyzed using the ZEN 2009 software (Carl Zeiss Microscopy GmbH). Calculations were carried out based on independent H&E-stained images with  $n = 3$  for each data point; all data were reported as the mean and standard deviation.

To perform ED1 (CD 68) staining, the slides were deparaffinized and hydrated in the same way as with H&E staining. The slides were then immersed in 1  $\times$  HIER T-EDTA buffer (pH 9.0) and incubated at 130°C for 20 min before antigen recovery. After cooling at room temperature, the

slides were washed in PBS and blocked at 25°C for 60 min using PBS solution with 5% horse serum and 0.3% Triton X-100. The samples were then treated with ED1 antibodies (mouse anti-rat CD68) at a 1:500 dilution ratio in antibody diluent at 4°C for 12 h. The slides were washed with PBS and PBST (0.05% Tween-80 in PBS), then treated with secondary antibodies (Alexa Fluor 594 goat anti-mouse IgG) at a 1:500 dilution ratio in antibody diluent at room temperature for 3 h. The samples were then washed with PBS and PBST, then treated with a 1 µg/mL DAPI solution. After thoroughly washing the samples with DW, the slides were mounted using a mounting solution. The stained slides were then visualized using a slide scanner (ZEISS Axio Scan. Z1; Carl Zeiss Microscopy GmbH). The quantitative evaluation of the stained images was performed with  $n = 3$  for each data point using the Image J program.

### 2.10. Statistical analyses

All data associated with *in vitro* hMSCs proliferation, *in vivo* compressive modulus, and number of ED1-positive cells on the printed scaffold were obtained from three independent experiments and were presented as the mean  $\pm$  standard deviation. To evaluate significance, the results were subjected to one-way analysis of variance coupled with Bonferroni's multiple-comparison correction using the SPSS 12.0 software (SPSS Inc., Chicago, IL, USA).

## 3. Results and discussion

### 3.1. Preparation of aliphatic PBC

In a previous report [27], we described the successful preparation of high-molecular-weight PBC via the bulk polycondensation of 1,4-butanediol and dimethyl carbonate using a small amount of sodium alkoxide

(0.2 mol % per 1,4-butanediol) as a catalyst. In our  $^1\text{H}$  NMR analyses, the peaks associated with  $-\text{CH}_2\text{O}-$  and  $-\text{CH}_2\text{CH}_2\text{O}-$  signals were observed at 4.5–4.1 and 2.1–1.7 ppm, respectively (Fig. 2a). The obtained PBC had a weight-average molecular weight of 104 kD and a polydispersity index of 2.2 in GPC (Fig. 2d).

Polymers used as a printing ink for printing generally occur in either solid or liquid form. Solid polymers can be easily melted in the heating chamber of FDM printers, after which they can be easily extruded from the nozzle of the FDM printer in their liquid form.

According to our DSC measurements, PBC exhibited a melting temperature of 150°C, indicating a semicrystalline state (Fig. 2b). The melting temperature of PBC indicated that this compound could be melted above 150°C in the heating chamber of the printer and could thus be effectively used as a printing ink. Our TGA analyses indicated that PBC experienced a 5% weight change due to decomposition at 308°C (Fig. 2c). These results indicated that the optimal printing temperature of PBC ranges between  $\geq 150^\circ\text{C}$  and  $\leq 300^\circ\text{C}$ .

Furthermore, the thermal stability of PBC was examined by incubation at 150–240°C for 30 min and 6 h. PBC exhibited no change in GPC under 200°C for 6 h, thus highlighting its thermal stability (Fig. 2e and f). Regarding color changes, PBC remained white below 200°C for 6 h but gradually changed to yellowish and brown above 220°C.

Collectively, these results indicated that PBC showed solid–liquid phase change at low and high temperature for FDM printing and printing condition of PBC should be set within maximum 4 h and below 200°C in the heating chamber to use as printing ink.

### 3.2. Evaluation of printability of PBC ink

In this study, the printability of PBC was assessed using FDM 3D printing. Ink must first melt in the heating chamber of the FDM printer,

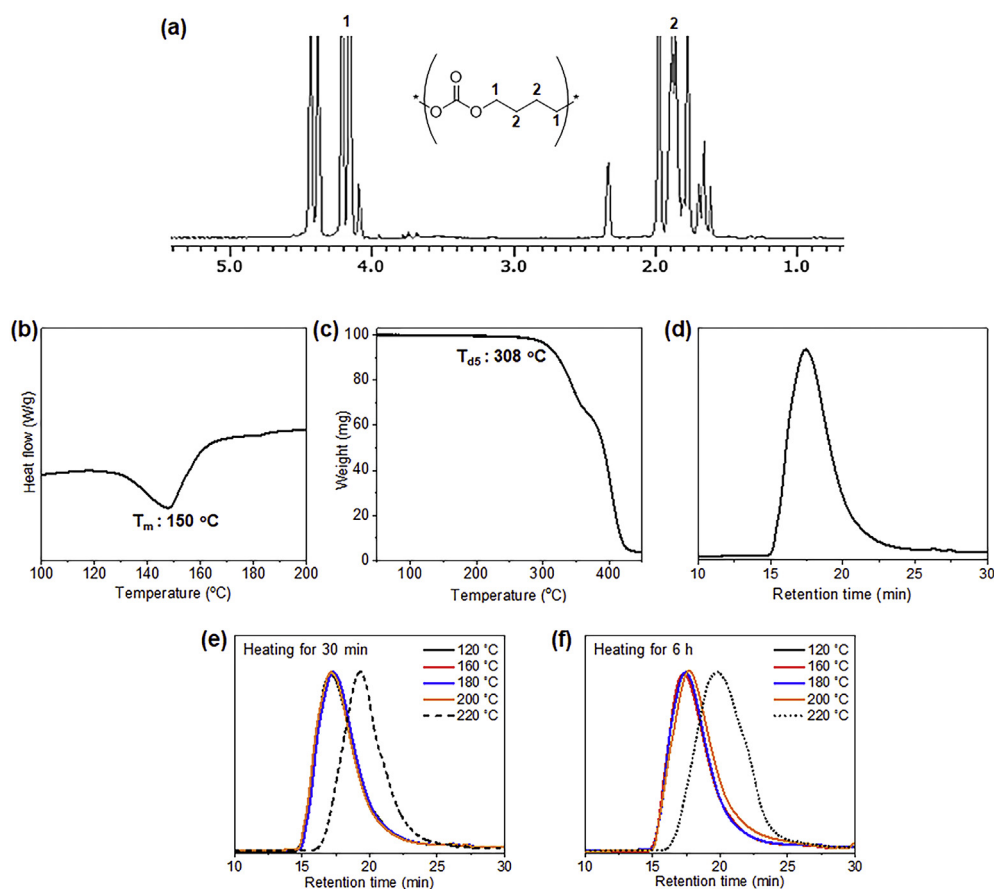


Fig. 2. Characterization of PBC. (a)  $^1\text{H}$  NMR spectra, (b) DSC curves, and (c) TGA curve, and (d) GPC of original PBC. GPC of PBC after heating for (e) 30 min and (f) 6 h at each temperature.

then flow from the printing nozzle on applying pressure and solidify to create a 3D scaffold structure at a given temperature (typically room temperature). Therefore, the effects of printing speed, chamber temperature, and extrusion pressure variations on the printability of PBC were also examined herein.

Three-dimensional plotting printability was first examined in terms of flowability from the micronozzle and solidification on the printing plate at room temperature after scaffold printing. Then, in the printer program, the line diameter and x-y length of the scaffold were set to  $400\ \mu\text{m}$  and  $450 \times 450\ \mu\text{m}^2$ , respectively.

First, we evaluated the PBC printability at different printing speeds (10, 15, and 20 mm/s) but a constant line shift of 0% at  $180^\circ\text{C}$  and 300 kPa (Fig. 3a). After FDM printing, the line diameter and x-y length of the printed scaffold were individually measured. The line diameter thickness of the printed scaffold increased at a 10 mm/s speed; however, the x-y pore length of the scaffold decreased due to the large flow of PBC ink per unit of time from the micronozzle when operated at a slow speed. In contrast, the scaffold printed at a 20 mm/s speed exhibited a decreased line diameter thickness and increased x-y pore length, indicating that high-speed printing resulted in less ink flow per unit of time from the micronozzle, thus decreasing the line diameter thickness of the printed scaffold and increasing the x-y length of the scaffold. Furthermore, the scaffold printed at a printing speed of 15 mm/s,  $180^\circ\text{C}$ , and 300 kPa matched the programmed line diameter and x-y length of the printed scaffold.

Next, the extrusion pressure was fixed to 300 kPa, and the temperature of the heating chamber was gradually increased from  $150^\circ\text{C}$  to  $240^\circ\text{C}$  (Fig. 3b). PBC did not completely melt below approximately  $160^\circ\text{C}$  in the heating chamber and thus failed to be extruded. However, the compound could be melted and extruded from the micronozzle at

$170^\circ\text{C}$ , albeit with some degree of discontinuity, indicating that this temperature range was not suitable for printing.

Above  $180^\circ\text{C}$ , the PBC exhibited good flowability from the micronozzle and appropriate solidification time for layer-by-layer printing. In addition, the printed scaffold exhibited a constant thickness and a smooth surface, thus highlighting the good printability of PBC when used as a printing ink for scaffold printing under the conditions specified herein. In contrast, at temperatures above  $220^\circ\text{C}$ , the printed scaffold appeared over melted and exhibited a yellow discoloration. This was likely because of the decomposition of the PBC during FDM printing caused by the high temperature.

Next, we examined the PBC printability at different line shift ratios of 0%, 25%, and 50% at  $180^\circ\text{C}$  and a 15 mm/s printing speed (Fig. 3c and Fig. S1). The scaffold exhibited the shape of the line movement according to the shift ratios, thus changing the shape and dimensions of the inter-layer pore.

Finally, we compared the PBC printability at different extrusion pressures (100–500 kPa) at  $180^\circ\text{C}$  and  $200^\circ\text{C}$  and at the same printing speed of 15 mm/s and the same line shift of 0% (Fig. 3d). The scaffold was programmed with same line diameter and x-y length as before and then individually measured to evaluate the PBC printability. As extrusion pressure increased, the line diameter thickness of the printed scaffold increased accordingly (Fig. 3e). The scaffold printed at  $200^\circ\text{C}$  exhibited an increased line diameter thickness compared with those at  $180^\circ\text{C}$ . Here, the scaffold printed at 300 kPa and  $180^\circ\text{C}$  and at 200 kPa and  $200^\circ\text{C}$  matched the programmed line diameter almost flawlessly (Fig. 3f).

Collectively, our findings indicated that the PBC ink in the FDM printer was affected by the variations in the extrusion pressures and temperature of the heating chamber. Based on these results, all scaffolds for downstream experiments were printed at  $180^\circ\text{C}$  and 300 kPa.

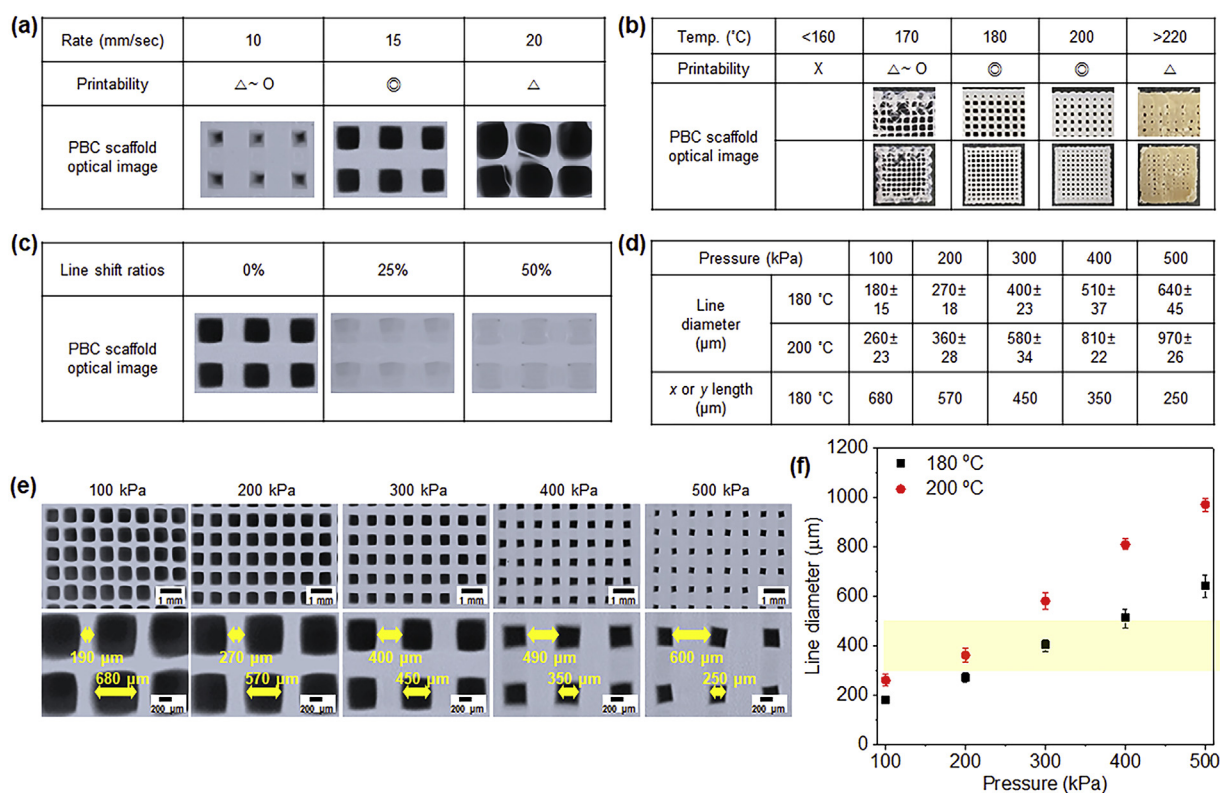


**Fig. 3.** Printability of PBC as a ink using fused deposition modeling (FDM) 3D printing. Printability at (a) different printing speeds (10, 15, and 20 mm/s) with a constant line shift of 0% at  $180^\circ\text{C}$  and 300 kPa and images of the printed scaffolds, (b) different temperatures ( $160$ – $220^\circ\text{C}$ ) with a constant line shift of 0% at 300 kPa and images of the printed scaffolds at  $170^\circ\text{C}$ ,  $180^\circ\text{C}$ ,  $200^\circ\text{C}$ , and  $220^\circ\text{C}$ , (c) different line shift ratios of 0%, 25%, and 50% with a 15 mm/s printing speed at  $180^\circ\text{C}$  and images of the printed scaffolds, (d) the determined line diameter and pore (x-y) of the scaffold printed as a function of printer pressure (100–500 kPa) at  $180^\circ\text{C}$  and  $200^\circ\text{C}$ , (e) images of the printed scaffolds [line diameter and pore (x-y)] of PBC scaffold printed at  $180^\circ\text{C}$  and each pressure, and (f) plot of line diameter of the printed scaffold vs. different pressures at  $180^\circ\text{C}$  and  $200^\circ\text{C}$ .

### 3.3. Evaluation of *in vitro* cell viability on printed PBC scaffolds

The printed PBC scaffold must provide a substrate for adhesion and proliferation of cells as a preliminary step to ensure the integration of the scaffold with the surrounding tissue. Although several cell types could be used to assess cell viability, hMSCs were chosen because the printed PBC scaffold will ultimately be applied to humans.

The PBC scaffolds printed at different line shift ratios of 0%, 25%, and 50% were used to assess cell viability. Afterward, hMSCs were cultured on the printed PBC scaffold and then monitored optical density using WST-1 assays throughout a 7-day incubation period to calculate the relative hMSC ratios through comparison with identical experiments on culture plate (control group; Fig. 4a and Fig. S2).

The viability of the hMSCs on all printed scaffolds was approximately 40–73% compared with the control group on day 1. The relative ratio of adherent hMSCs on PBC scaffolds increased for 7 days at largely similar rates according to the culture time and with increasing of line shift ratios, indicating a gradual proliferation of the hMSCs on PBC scaffolds.

At 7 days, the relative ratios of adherent hMSCs on PBC scaffolds printed at line shift ratio (50%) were ~80% of that on the control group, whereas the relative ratios of adherent hMSCs on PBC scaffolds printed at line shift ratio (0%) were ~45% of that on the control group. This was probably because of the line shift in the scaffold allowed for easy penetration of hMSCs throughout the scaffold network.

Nevertheless, our findings demonstrated that hMSCs can attach and proliferate on the scaffolds designed herein, although in comparison to WST-1 assay of hMSCs, the adhesion and proliferation of hMSCs on all printed scaffolds were observed to be lower than that of culture plates.

SEM was used to visualize the hMSCs on the printed PBC scaffold (Fig. 4b). hMSCs were uniformly distributed throughout the entire area of the printed scaffold surface. Most of the attached hMSCs were round on day 1. However, on Days 4 and 7, the hMSCs formed cytoplasmic extensions on the surface of the printed scaffold, and the filopodia of the hMSCs became anchored to the surface of the printed scaffold.

Collectively, these results suggest that hMSCs grew well on the surface of the printed PBC scaffold. These findings indicated that the printed PBC scaffolds had an adequate biocompatibility *in vitro* and were thus fabricated for subsequent *in vivo* experiments.

### 3.4. *In vivo* implantation of printed PBC scaffold

PBC scaffolds (10 mm width × 10 mm length × 3 mm height) were printed with a 400 μm line strand size and a 450 × 450 μm<sup>2</sup> pore size to conduct *in vivo* experiments. Afterward, the printed PBC scaffolds were transplanted subcutaneously on the back of SD rats and monitored for 16 weeks to assess their biocompatibility and biodegradability (Fig. 5a). The rats transplanted with the printed PBC scaffolds exhibited no abnormal symptoms such as self-harm, vomiting, or weight loss.

The PBC scaffold was then extracted at predetermined times (Fig. 5b). The extracted PBC scaffold maintained its original shape at 4–16 weeks. Fig. 5c and d illustrate the changes in line thickness and x-y length of PBC scaffold according to implantation time.

In the magnified Camscope images (Fig. 5d), the PBC scaffold exhibited a gradual increase in tissue and blood vessels as implantation time increased. In addition, in the cross-sectional SEM images of the transplanted PBC scaffold (Fig. 5e), the spherical images of the line in the cross-section of the printed PBC indicated a gradual structural collapse and decreased thickness as implantation time increased. Therefore, we concluded that the printed PBC scaffold was gradually degraded with implantation time.

### 3.5. *In vivo* physicochemical properties of the implanted printed PBC scaffold

Developing printing ink using new PBC polymers requires *in vivo* evaluation, including the assessment of ink biodegradation, the structural and mechanical properties of the scaffold, and neotissue formation. Therefore, the physicochemical properties of the removed scaffolds were subsequently evaluated as a function of implantation time.

To assess *in vivo* degradation, the extent of degradation of the PBC scaffold extracted from SD rats biopsied at different time points over 4, 8, and 16 weeks was monitored via <sup>1</sup>H NMR, GPC, and compressive modulus analyses (Fig. 6).

The <sup>1</sup>H NMR spectra of the PBC scaffold were measured before and after *in vivo* implantation (Fig. 6a and b). The spectra exhibited peaks that were attributed to degraded oligomeric PBC and butylene derivatives, as well as the parent PBC observed after 4 weeks of degradation (Fig. 6c), all of which increased with implantation time.

Here, the peaks that characterize degraded oligomeric PBC and butylene derivatives were obtained from the soluble portions in *n*-hexane and ether. Furthermore, the characteristic peaks of the parent PBC were also observed in the insoluble portions in *n*-hexane and ether.

The GPC of the PBC scaffold exhibited a slight low-molecular-weight peak ascribed to degradation at 4 weeks (Fig. 6d). Furthermore, the intensity of the peaks decreased gradually as implantation time increased. At 8 and 16 weeks, however, the peaks were observed at similar positions, indicating that molecular weight became constant with time.

Next, the normalized degradation from MW and line diameter of the PBC scaffold and *in vivo* neotissue formation were plotted as a function of implantation time (Fig. 6e). The MW degradation and line diameter of the PBC scaffold decreased as implantation time increased.

The extent of *in vivo* neotissue formation was calculated and plotted at implantation and on the designated weeks. The neobone tissues increased from 0 to 40%, 45%, and 75% at 4, 8, and 16 weeks, respectively. This result indicated that the PBC scaffold can gradually biodegrade over time, after which the tissue filled the degraded area of the scaffold.

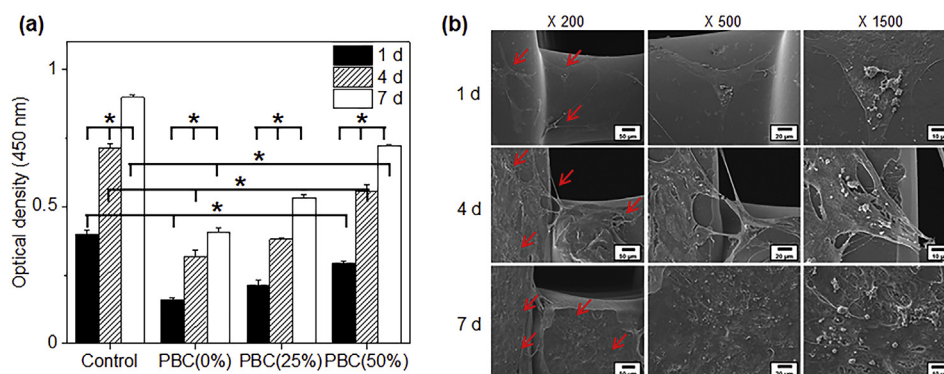


**Fig. 4.** Viability of hMSCs grown on printed PBC scaffolds with different line shift ratios (0%, 25%, and 50%). (a) WST-1 assay of hMSCs grown on culture plates and printed PBC scaffolds for 1, 4, and 7 days (\**p* < 0.01). (b) SEM images of hMSCs grown on printed PBC scaffolds for 1, 4, and 7 days.

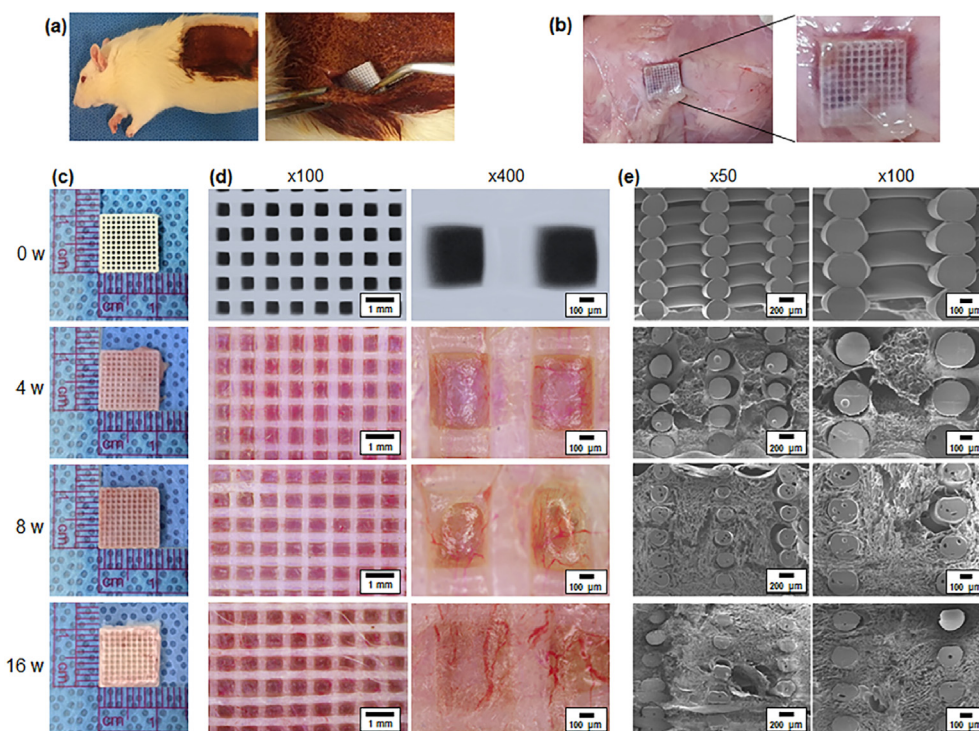


**Fig. 5.** *In vivo* implantation of printed PBC scaffold (Week 0 represents the original PBC scaffold). (a) Subcutaneous implantation of PBC scaffold to Sprague-Dawley (SD) rats, (b) photographs of *in vivo* PBC scaffold sacrificed at 16 weeks, (c) photographs of *in vivo* PBC scaffold removed at each time, (d) Camscope image of PBC scaffold (100 $\times$ , 400 $\times$ ), and (e) SEM image of PBC scaffolds removed from SD rats at 4, 8, and 16 weeks after implantation (50 $\times$ , 100 $\times$ ).

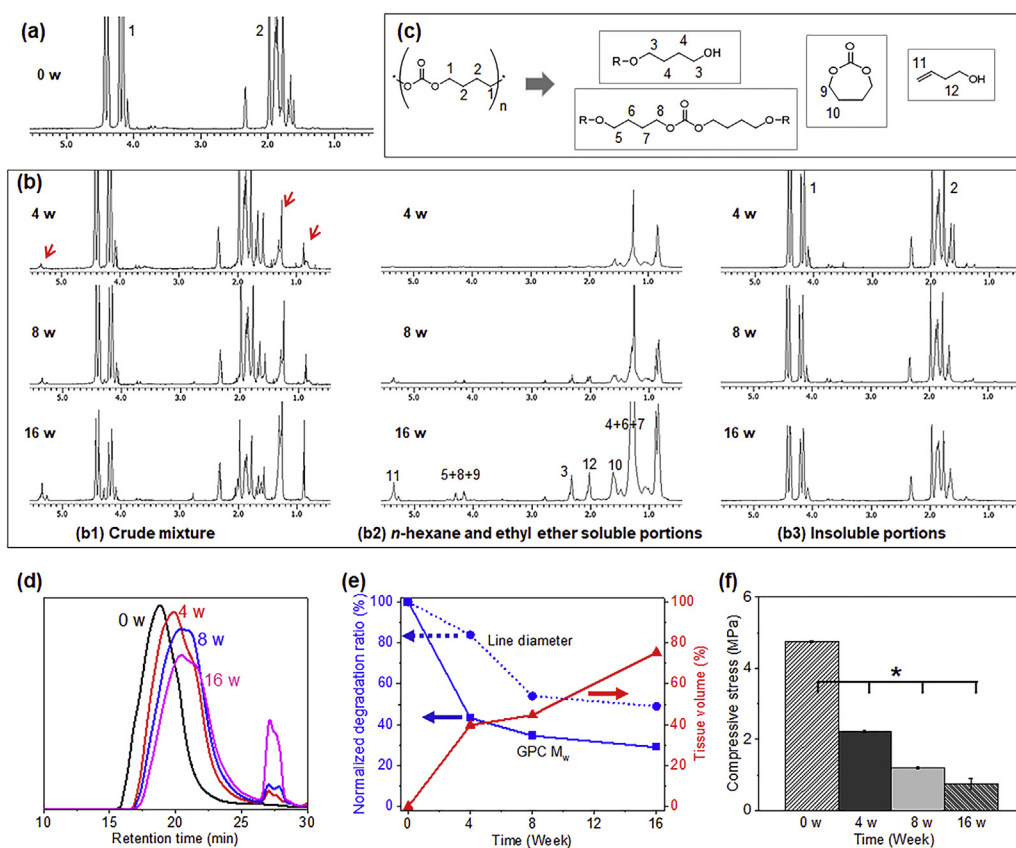


**Fig. 6.** *In vivo* physicochemical properties of implanted PBC scaffold (Week 0 represents the original PBC scaffold).  $^1\text{H}$  NMR spectra of PBC scaffold (a) before and (b) after degradation, (b1) crude mixture before separation, (b2) soluble, and (b3) insoluble portions in *n*-hexane and ethyl ether. (c) Plausible degradation mechanism of PBC. (d) Changes in the GPC curve of PBC scaffold removed from SD rats at 4, 8, and 16 weeks after implantation. (e) Time since implantation vs. the normalized degradation of the implanted PBC scaffold based on the GPC signals (line blue), the normalized degradation from line diameter of the implanted PBC scaffold (dot line blue), and tissue volume (line red) calculated after H&E staining (as shown in Fig. 7). (f) Compressive stress at 10% strain of PBC scaffold removed from SD rats at 4, 8, and 16 weeks after implantation ( $*p < 0.01$ ). (For interpretation of the references to color/colour in this figure legend, the reader is referred to the Web version of this article.)

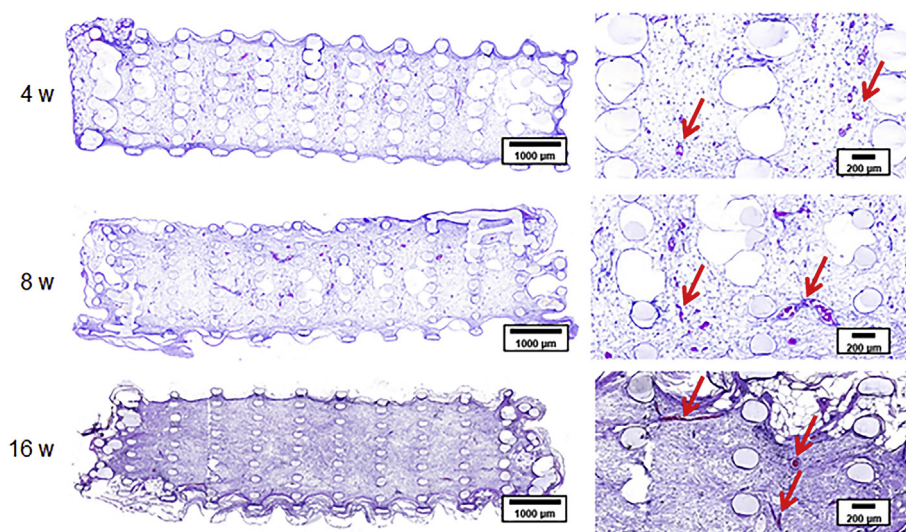


**Fig. 7.** H&E-stained histological sections of PBC scaffolds removed from SD rats at 4, 8, and 16 weeks after implantation. Blood vessels are indicated by arrows.

The compressive modulus of the printed PBC scaffold was 4.8 MPa before implantation (Fig. 6f and Fig. S3). The compressive strength was 2.2 MPa at 4 weeks, 1.2 MPa at 8 weeks, and 0.8 MPa at 16 weeks, showing a rapid decrease. We speculated that the rapid decrease in compressive strength was caused by the collapse in the 3D structure of the PBC scaffolds, as demonstrated by our SEM observations (Fig. 5e).

According to our findings, PBC ink enables the printing of 3D PBC scaffolds whose gradual change of mechanical properties depends on the gradual biodegradation rate during *in vivo* neotissue formation.

### 3.6. Histological evaluation of *in vivo* implantation of printed PBC scaffold

To assess the *in vivo* biocompatibility of the printed PBC scaffolds, fixed tissue sections from the implanted PBC scaffolds excised at the designated week were examined using histological H&E staining (Fig. 7). H&E staining indicated that the *in vivo* neotissue formation inside the scaffold increased over time. In addition, we observed an empty space because of the cross-sectional line of the scaffold, which became gradually crushed due to biodegradation. This trend was similar to decreasing line thickness of the scaffold in the cross-section visualized via SEM analysis (Fig. 5e). Additionally, new blood vessel formation was observed in the pores inside the PBC scaffold, which also increased with implantation time.

The extent of host cell infiltration and inflammatory cell accumulation within and surrounding the printed PBC scaffolds were characterized by staining the tissue with ED1 (red) to identify macrophages, whereas nuclei were stained with DAPI (blue) (Fig. 8a). DAPI staining revealed the presence of numerous host cells within and surrounding the PBC

scaffold. ED1 staining showed that macrophages were present in the pore and surrounding the PBC scaffold. The ED1-positive cells were counted and normalized by the total stained tissue area to determine the extent of inflammation (Fig. 8b). The number of macrophages (ED1-positive cells) significantly decreased at longer times postimplantation. This response was less pronounced than the response to Poly(L-lactide-co-glycolide) (PLGA) and Poly(caprolactone-co-L-lactide) (PCLA) [28–30], which substantially promotes the infiltration of macrophages and neutrophils.

## 4. Discussion

Several biomaterial inks have been recently used to produce engineered tissues or organs using 3D printing [2–7]. Furthermore, FDM is one of the most popular processes to create scaffolds using several biomaterial inks [8–10]. However, FDM 3D printing inks must meet certain critical characteristics, including high reproducibility and the ability to render scaffolds with precise shape fidelity in an automated manner. Moreover, scaffolds fabricated by 3D printing inks must be biocompatible, safe, and nonimmunogenic, in addition to having a biodegradation period consistent with the appropriate time for regeneration of the tissue or entire organ.

Several biomaterials are available as 3D printing inks for scaffold printing, including biodegradable polyesters such as poly-L-lactide, polyglycolide (PGA; or their PLGA co-polyesters), and polycaprolactone (PCL) [13].

PCL is one of the most widely used printing inks for FDM-based 3D printing; however, the slow degradation kinetics of this ink (2–4 years) make it unsuitable for use in biodegradable implants [31]. PLLA is

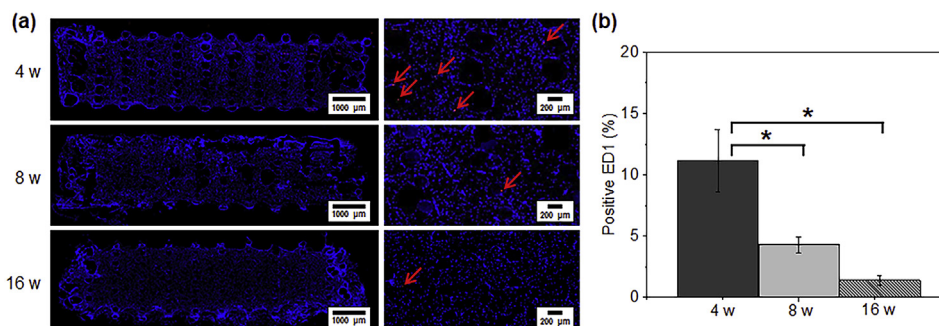


**Fig. 8.** Immunofluorescence ED1 staining of *in vivo* implantation of the printed PBC scaffolds. (a) Immunofluorescence ED1-stained histological sections and (b) number of ED1-positive cells of PBC scaffold removed from SD rats at 4, 8, and 16 weeks after implantation (\* $p < 0.01$ ). The arrows indicate the ED1-positive cells.

another popular printing ink, and scaffolds printed with PLLA can gradually biodegrade inside the body within 6 months to 2 years [32]. Furthermore, we reported the feasibility of PLLA-co-PGA-co-PCL (PLGC) and PCL-co-PLLA (PCLA) copolymer with various proportions of PLLA, PGA, and PCL printing inks for FDM 3D printing [28,33]. The printed PLGC and PCLA scaffolds were ideally tailored to match a tissue regeneration rate of up to 12 weeks, as they exhibited a molecular weight half-life of 8 weeks.

Park et al. recently printed baby toys via FDM using a poly(isosorbide carbonates) ink derived from corn starch at 270°C and examined whether this material could be used as an environmentally friendly alternative to petrochemical-derived polycarbonates in *ex vivo* applications [34].

To the best of our knowledge, few studies have documented the 3D printing of polycarbonate scaffolds using FDM printing. However, several studies have described the 3D printing of polycarbonate scaffolds using DLP/SLS [35,36].

In the case of DLP/SLS, polycarbonate inks with specific functional groups are required for the photoreaction and photoactive initiator. In addition, the printed scaffolds often contain unreacted photofunctional groups or photoinitiators and therefore may cause *in vivo* toxicity in bioapplications. In contrast, FDM printing is a much more straightforward thermal-based approach, and residual unreacted materials pose no substantial threats.

In this study, we prepared aliphatic PBC with melting temperatures of 150°C, which easily melted in the heating chamber at  $\geq 150^\circ\text{C}$  during the FDM processing, after which we examined biodegradable PBC as a printing ink for FDM. First, we evaluated the effect of several factors on PBC printability during FDM processing, including line shift ratios, chamber temperature, and extrusion pressure. Under optimized conditions, the melted PBC exhibited easy mobility from the micronozzle and solidification at ambient temperature, both of which facilitated its layer-by-layer extrusion.

Collectively, our findings demonstrated the feasibility of PBC as printing ink for scaffold fabrication with quick turn-around and high reproducibility using FDM. More importantly, this study was the first to assess PBC as a printing ink for *in vivo* application.

During the scaffold fabrication process, porous scaffolds are required for the ingrowth of the tissue and vascularization to avoid hypoxia and construct failure. Therefore, porosity must be designed in all directions. It has been reported that the effective pore size for tissue-engineered scaffolds is 20–1,500  $\mu\text{m}$  [37,38]. Although we did not design suitable pores based on both tissue ingrowth and mechanical properties using PBC scaffolds, we obtained precisely printed scaffolds with a line diameter of 400  $\mu\text{m}$  and x-y length of  $450 \times 450 \mu\text{m}^2$ . In addition, we successfully obtained a PBC scaffold that could be tuned and optimized because of the good printability of the PBC ink. Furthermore, we fabricated several organ shapes using PBC ink, as 3D printing is a state-of-the-art technology that enables the fabrication of organs with a hierarchical architecture similar to that of their native counterparts (Fig. S4).

Similar to PBC ink printability, once the *in vivo* physicochemical properties (e.g., biodegradation) of the printed PBC scaffolds are well understood, PBC scaffolds can be printed using a PBC ink tailored to specific clinical applications. Therefore, we examined the *in vivo* biodegradation and compressive modulus of the printed PBC scaffold alone to examine its *in vivo* physicochemical properties for 16 weeks.

There have been several reports regarding the surface erosion degradation of *in vivo* implanted poly(ethylene carbonate) and poly(trimethylene carbonate) from the activity of adherent macrophages and foreign body giant cells rather than acid/base-catalyzed hydrolysis [24, 39]. The *in vivo* implanted PBC scaffolds can degrade the butanediols and carbon dioxide as the degradation products. The carbon dioxide forms carbonic acid through reaction with water, but this is a weak acid, with a pKa of 6.35 [40], and therefore, acid-catalyzed hydrolysis is not a significant contributing factor.

Moreover, the MW of the printed PBC scaffold remained largely constant at 8 and 16 weeks after a change in MW at 4 weeks according to

GPC. We also identified a large amount of PBC parent peaks after 16 weeks in the NMR spectra. In addition, the removed PBC scaffold largely retained its shape even after 16 weeks compared with the scaffold at Week 0. However, the line of the PBC scaffold degraded uniformly with time. This suggests that the inside of the PBC scaffolds does not degrade until all the surrounding PBC has been degraded. This, in turn, indicated that the *in vivo* implanted PBC scaffolds degraded from the exterior surface of the printing line. Collectively, these findings indicated that the PBC scaffold undergoes surface erosion when used for *in vivo* applications.

The printed PBC scaffold exhibited compressive moduli at approximately 4.8 MPa, which is considered to be suitable for most soft tissues (0.4–350 MPa) [41]. The compressive moduli of the printed PBC scaffold decreased as implantation time increased. This change in the *in vivo* intrinsic compressive moduli of the printed PBC scaffold can be used for future specific tissue engineering with regenerative cells or biological factors.

The printed scaffold for *in vitro* and *in vivo* applications must be highly biocompatible. In this study, we selected hMSCs because they are currently being applied in regenerative medicine. The hMSCs exhibited good adhesion and proliferation on the printed PBC scaffold, indicating good biocompatibility. However, given that this study only evaluated the *in vitro* biocompatibility of the printed PBC scaffold, we are currently examining cranial bone regeneration using printed PBC scaffolds with hMSCs and will be reporting these findings in future publications.

Staining with H&E revealed the neotissue formation surrounding the printed PBC scaffolds. Over time, however, there was a marked increase in neotissue formation. Our findings demonstrated infiltration by and ingrowth of host cells, along with adequate engraftment of the printed PBC scaffold within the host tissue, suggesting that these printed PBC scaffolds may be biocompatible *in vivo*.

To the best of our knowledge, there have been few previous efforts to examine host tissue responses to printed scaffolds similar to our experiments using immunohistochemical staining with the macrophage marker ED1. Although the exact time taken to understand the inflammatory response for printed scaffolds is not determined, recently, we compared the *in vivo* inflammation of salt-leached and printed PCLA scaffolds at 16 weeks [28]. The printed PCLA scaffolds contained slightly more ED1-positive cells than the salt-leached PCLA scaffolds. Therefore, we concluded that the *in vivo* inflammation of scaffolds might depend on the porosity and morphology of the scaffolds, as well as their *in vivo* duration [42].

Based on simple comparisons of printed PCLA and PBC scaffold during the same implantation time, although there are differences in the pore and line diameter of the scaffold, the printed PBC scaffold induced weaker inflammatory responses than those of printed PCLA. We thus concluded that the *in vivo* implanted PBC scaffolds degraded to butanediols and carbon dioxide, which are relatively noninflammatory materials, whereas *in vivo* implanted printed PCLA scaffolds eventually degraded directly to acid, leading to a slightly stronger inflammation reaction.

Taken together, our findings indicated that the printed PBC scaffolds were biocompatible *in vivo* and induced *in vivo* neotissue formation with minor host tissue responses, demonstrating that PBC could be used as a suitable printing ink candidate for the creation of scaffolds via FDM printing.

## 5. Conclusion

Our findings demonstrated the feasibility of PBC ink for FDM printing depending on the speed, temperature, and pressure of the FDM printer. The printed PBC scaffolds exhibited *in vivo* biocompatibility and biodegradability for a defined experimental period and induced only a modest inflammatory response. Therefore, PBC may potentially be used as a biocompatible and biodegradable ink for the generation of scaffolds using an FDM printer. Our findings demonstrate the promising potential of PBC ink as a state-of-the-art technology that enables the fabrication of

several organ shapes with a hierarchical architecture as a viable alternative to *ex vivo* printed scaffolds. A more detailed study on cranial bone regeneration using printed PBC scaffolds and hMSCs is currently being conducted.

### Authors' contributions

Y.B.J., J.Y.P., and M.S.K. contributed to methodology. J.Y.P. and M.S.K. contributed to conceptualization. Y.B.J., Y.K., S.L., and H.J.H. contributed to formal analysis. Y.B.J., Y.K., S.L., and H.J.H. contributed to visualization. Y.B.J., Y.K., S.L., H.J.H., and S.C. contributed to validation. B.Y.L. and M.S.K. contributed to project administration. B.Y.L. and M.S.K. contributed to supervision. S.C. and M.S.K. contributed to funding acquisition. Y.B.J. wrote the original article. M.S.K. reviewed and edited the article. All authors have read and agreed to the published version of the article.

### Funding

This study was supported by the National Research Foundation of Korea (NRF) grants, Creative Materials Discovery Program (2019M3D1A1078938), and Priority Research Centers Program (2019R1A6A1A11051471).

### Declaration of competing interest

The authors declare that they have no known competing financial interests or personal relationships that could have appeared to influence the work reported in this paper.

### Appendix A. Supplementary data

Supplementary data to this article can be found online at <https://doi.org/10.1016/j.mtbio.2021.100129>.

### References

- [1] P. Rashidi, A. Bihorac, Artificial intelligence approaches to improve kidney care, *Nat. Rev. Nephrol.* 16 (2) (2020) 71–72.
- [2] W. Li, L.S. Mille, J.A. Robledo, T. Uribe, V. Huerta, Y.S. Zhang, Recent advances in formulating and processing biomaterial inks for vat polymerization-based 3D printing, *Adv. Healthc. Mater.* 9 (15) (2020), e2000156.
- [3] S. Mao, Y. Pang, T. Liu, Y. Shao, J. He, H. Yang, Y. Mao, W. Sun, Bioprinting of in vitro tumor models for personalized cancer treatment: a review, *Biofabrication* 12 (4) (2020), 042001.
- [4] E.S. Gargus, H.B. Rogers, K.E. McKinnon, M.E. Edmonds, T.K. Woodruff, Engineered reproductive tissues, *Nat. Biomed. Eng.* 4 (4) (2020) 381–393.
- [5] T. Bedir, S. Ulag, C.B. Ustundag, O. Gunduz, 3D bioprinting applications in neural tissue engineering for spinal cord injury repair, *Mater. Sci. Eng. C Mater. Appl.* 110 (2020) 110741.
- [6] N. Ashammakhi, S. Ahadian, C. Xu, H. Montazerian, H. Ko, R. Nasiri, N. Barros, A. Khademhosseini, Bioinks and bioprinting technologies to make heterogeneous and biomimetic tissue constructs, *Mater. Today Bio* 1 (2019) 100008.
- [7] J.W. Seo, S.R. Shin, Y.J. Park, H. Bae, Hydrogel production platform with dynamic movement using photo-crosslinkable/temperature reversible chitosan polymer and stereolithography 4D printing technology, *Tissue Eng. Regen. Med.* 17 (2020) 42–431.
- [8] M.A. Heinrich, W. Liu, A. Jimenez, J. Yang, A. Akpek, X. Liu, Q. Pi, X. Mu, N. Hu, R.M. Schiffelers, J. Prakash, J. Xie, Y.S. Zhang, 3D bioprinting: from benches to translational applications, *Small* 15 (23) (2019), e1805510.
- [9] N. Hossain, M.A. Chowdhury, M.B.A. Shuvo, M.A. Kashem, M. Kchaou, 3D-printed objects for multipurpose applications, *J. Mater. Eng. Perform.* (2021) 1–12.
- [10] X. Cui, J. Li, Y. Hartanto, M. Durham, J. Tang, H. Zhang, G. Hooper, K. Lim, T. Woodfield, Advances in extrusion 3D bioprinting: a focus on multicompartment hydrogel-based bioinks, *Adv. Healthc. Mater.* 9 (15) (2020), e1901648.
- [11] F. Liu, X. Wang, Synthetic polymers for organ 3D printing, *Polymers* 12 (2020) 1765.
- [12] S. Heid, A.R. Boccaccini, Advancing bioinks for 3D bioprinting using reactive fillers: a review, *Acta Biomater.* 113 (2020) 1–22.
- [13] T. Ahlfeld, V. Guduric, S. Duin, A.R. Akkineni, K. Schütz, D. Kilian, J. Emmermacher, N. Cubo-Mateo, S. Dani, M.V. Witzleben, J. Spangenberg, R. Abdelgaber, R.F. Richter, A. Lode, M. Gelinsky, Methylcellulose - a versatile printing material that enables biofabrication of tissue equivalents with high shape fidelity, *Biomater. Sci.* 8 (8) (2020) 2102–2110.
- [14] Z. Wan, P. Zhang, Y. Liu, L. Lv, Y. Zhou, Four-dimensional bioprinting: current developments and applications in bone tissue engineering, *Acta Biomater.* 101 (2020) 26–42.
- [15] J. Groll, J.A. Burdick, D.W. Cho, B. Derby, M. Gelinsky, S.C. Heilshorn, T. Jüngst, J. Malda, V.A. Mironov, K. Nakayama, A. Ovsianikov, W. Sun, S. Takeuchi, J.J. Yoo, T.B.F. Woodfield, A definition of bioinks and their distinction from biomaterial inks, *Biofabrication* 11 (2019), 013001.
- [16] S. Bandari, D. Nyavanandi, N. Dumpa, M.A. Repka, Coupling hot melt extrusion and fused deposition modeling: critical properties for successful performance, *Adv. Drug Deliv. Rev.* 172 (2021) 52–63.
- [17] G.G. Pereira, S. Figueiredo, A.I. Fernandes, J.F. Pinto, Polymer selection for hot-melt extrusion coupled to fused deposition modelling in pharmaceuticals, *Pharmaceutics* 12 (9) (2020) 795.
- [18] D. Sooriyaarachchi, H.J. Minière, S. Maharubin, G.Z. Tan, Hybrid additive microfabrication scaffold incorporated with highly aligned nanofibers for musculoskeletal tissues, *Tissue Eng. Regen. Med.* 16 (1) (2019) 29–38.
- [19] J. Long, H. Gholizadeh, J. Lu, C. Bunt, A. Seyfoddin, Application of fused deposition modelling (FDM) method of 3D printing in drug delivery, *Curr. Pharm. Des.* 23 (3) (2017) 433–439.
- [20] L. Papadimitriou, P. Manganas, A. Ranella, E. Stratakis, Biofabrication for neural tissue engineering applications, *Mater. Today Bio* 6 (2020) 100043.
- [21] R.P. Brannigan, A.P. Dove, Synthesis, properties and biomedical applications of hydrolytically degradable materials based on aliphatic polyesters and polycarbonates, *Biomater. Sci.* 5 (1) (2016) 9–21.
- [22] S. Tempelaar, L. Mespouille, O. Coulembier, P. Dubois, A.P. Dove, Synthesis and post-polymerisation modifications of aliphatic poly(carbonate)s prepared by ring-opening polymerisation, *Chem. Soc. Rev.* 42 (3) (2013) 1312–1336.
- [23] S.Y. Park, J. Chun, J.Y. Yeon, P.C. Lee, Y. Hwang, B.G. Song, R. Ramos, C.Y. Ryu, B.Y. Lee, Branched poly(1,4-butylene carbonate-co-terephthalate)s: LDPE-like semicrystalline thermoplastics, *J. Polym. Sci. Part A Polym. Chem.* 53 (7) (2015) 914–923.
- [24] B. Amsden, In vivo degradation mechanisms of aliphatic polycarbonates and functionalized aliphatic polycarbonates, *Macromol. Biosci.* (2021), e2100085.
- [25] F. Oveissi, S. Naficy, A. Lee, D.S. Winlaw, F. Dehghani, Materials and manufacturing perspectives in engineering heart valves: a review, *Mater. Today Bio* 5 (2020) 100038.
- [26] W. Gruszka, J.A. Garden, Advances in heterometallic ring-opening (co) polymerisation catalysis, *Nat. Commun.* 12 (1) (2021) 3252.
- [27] J.H. Park, J.Y. Jeon, J.J. Lee, Y. Jang, J.H. Varghese, B.Y. Lee, Preparation of high-molecular-weight aliphatic polycarbonates by condensation polymerization of diols and dimethyl carbonate, *Macromolecules* 46 (9) (2013) 3301–3308.
- [28] D.Y. Kwon, J.Y. Park, B.Y. Lee, M.S. Kim, Comparison of scaffolds fabricated via 3D printing and salt leaching: in vivo imaging, biodegradation, and inflammation, *Polymers* 12 (2020) 2210.
- [29] M.S. Kim, H.H. Ahn, Y.N. Shin, M.H. Cho, G. Khang, H.B. Lee, An in vivo study of the host tissue response to subcutaneous implantation of PLGA- and/or porcine small intestinal submucosa-based scaffolds, *Biomaterials* 28 (34) (2007) 5137–5143.
- [30] S. Jilek, E. Walter, H.P. Merkle, B. Corthesy, Modulation of allergic responses in mice by using biodegradable poly(lactide-co-glycolide) microspheres, *J. Allergy Clin. Immunol.* 114 (4) (2004) 943–950.
- [31] H. Cui, M. Nowicki, J.P. Fisher, L.G. Zhang, 3D bioprinting for organ regeneration, *Adv. Healthcare Mater.* 6 (2017) 1601118.
- [32] L. Valot, J. Martinez, A. Mehdi, G. Subra, Chemical insights into bioinks for 3D printing, *Chem. Soc. Rev.* 48 (2019) 4049–4086.
- [33] D.Y. Kwon, J.S. Kwon, S.W. Shim, J.H. Park, J.H. Lee, J.H. Kim, W. Kim, M.S. Kim, Preparation of three-dimensional scaffolds by using solid freeform fabrication and feasibility study for the scaffolds, *J. Mat. Chem. B* 2 (2014) 1689–1698.
- [34] S.J. Park, J.E. Lee, J.H. Park, M. Lyu, K. Park, M.S. Koo, S.C. Jin, K.Y. Kim, Y. Son, FDM 3D printing of environmental friendly and high strength bio-based PC filaments for baby toys, *Elastom. Compos.* 52 (2017) 99–104.
- [35] Y. Wu, M.C. Simpson, J. Jin, Fast hydrolytically degradable 3D printed object based on aliphatic polycarbonate thiol-yne photoresins, *Macromol. Chem. Phys.* 22 (2021) 2000435.
- [36] A. Awad, F. Fina, A. Goyanes, S. Gaisford, A.W. Basit, 3D printing: principles and pharmaceutical applications of selective laser sintering, *Int. J. Pharm.* 586 (2020) 119594.
- [37] C.M. Murphy, M.G. Haugh, F.J. O'Brien, The effect of mean pore size on cell attachment, proliferation and migration in collagen-glycosaminoglycan scaffolds for bone tissue engineering, *Biomaterials* 31 (2010) 461.
- [38] S. Nehrer, H.A. Breinan, A. Ramappa, G. Young, S. Shortkroff, L.K. Louie, C.B. Sledge, I.V. Yannas, M. Spector, Matrix collagen type and pore size influence behaviour of seeded canine chondrocytes, *Biomaterials* 18 (1997) 769.
- [39] W. Yu, E. Maynard, V. Chiaradia, M.C. Arno, A.P. Dove, Aliphatic polycarbonates from cyclic carbonate monomers and their application as biomaterials, *Chem. Rev.* (2021), <https://doi.org/10.1021/acs.chemrev.0c00883>.
- [40] R.C. Weast, M.J. Astle, CRC Handbook of Chemistry and Physics, 62nd ed., CRC Press, Boca Raton, Florida, USA, 1983.
- [41] S. Hollister, Porous scaffold design for tissue engineering, *Nat. Mater.* 4 (2005) 518.
- [42] R. Sridharan, A.R. Cameron, D.J. Kelly, C.J. Kearney, F.J. O'Brien, Biomaterial based modulation of macrophage polarization: a review and suggested design principles, *Mater. Today* 18 (2015) 313–325.